Monthly Notices of the ROYAL ASTRONOMICAL SOCIETY
MNRAS **465,** 4650–4657 (2017)
Advance Access publication 2016 November 29
doi:10.1093/mnras/stw3082

On the progenitor of the Type IIb supernova 2016gkg

Charles D. Kilpatrick,[1★] Ryan J. Foley,[1] Louis E. Abramson,[2] Yen-Chen Pan,[1] Cicero-Xinyu Lu,[2] Peter Williams,[2] Tommaso Treu,[2] Matthew R. Siebert,[1] Christopher D. Fassnacht[3] and Claire E. Max[1]

[1] *Department of Astronomy and Astrophysics, University of California, Santa Cruz, CA 95064, USA*
[2] *Department of Physics and Astronomy, University of California, Los Angeles, CA 90095, USA*
[3] *Department of Physics, University of California, One Shields Avenue, Davis, CA 95616, USA*

Accepted 2016 November 24. Received 2016 November 17; in original form 2016 October 15

ABSTRACT

We present a detection in pre-explosion *Hubble Space Telescope* (*HST*) imaging of a point source consistent with being the progenitor star of the Type IIb supernova (SN IIb) 2016gkg. Post-explosion imaging from the Keck adaptive optics system was used to perform relative astrometry between the Keck and *HST* imaging. We identify a single point source in the *HST* images coincident with the SN position to 0.89σ. The *HST* photometry is consistent with the progenitor star being an A0 Ia star with $T = 9500$ K and $\log{(L/L_\odot)} = 5.15$. We find that the SN 2016gkg progenitor star appears more consistent with binary than single-star evolutionary models. In addition, early-time light-curve data from SN 2016gkg revealed a rapid rise in luminosity within $\sim$0.4 d of non-detection limits, consistent with models of the cooling phase after shock break-out. We use these data to determine an explosion date of 2016 September 20.15 and progenitor-star radius of $\log{(R/R_\odot)} = 2.41$, which agrees with photometry from the progenitor star. Our findings are also consistent with detections of other SNe IIb progenitor stars, although more luminous and bluer than most other examples.

Key words: stars: evolution – supernovae: general – supernovae: individual: SN 2016gkg.

1 INTRODUCTION

Any normal core-collapse supernova (SN) can yield valuable new insight into SN explosion mechanisms when its progenitor star is detected in pre-explosion imaging. The two canonical examples are SNe 1987A and 1993J, which revealed, among other aspects of SNe and their progenitor stars, that binary evolution is central to SNe (Aldering, Humphreys & Richmond 1994), that stars in the mass range 15–25 $M_\odot$ explode as SNe (Arnett et al. 1989; Podsiadlowski 1993; Maund et al. 2004), and that mass-transfer can describe both the hydrogen envelopes and circumstellar environments of some SNe (e.g. Morris & Podsiadlowski 2007; Weiler et al. 2007). Beyond these well-studied examples, roughly 20 progenitor systems have been identified and statistical studies of the connection between progenitor stars and SNe are now possible (Smartt et al. 2009; Smartt 2015). Of particular interest is the luminosity and colour distribution of these progenitor stars and inferences about their physical properties. Apart from notable examples such as SN 1987A and SN 2009ip (e.g. Arnett 1987; Woosley et al. 1987; Mauerhan et al. 2013, with more studies since), virtually all SN progenitor stars have $B - V > 0.3$ mag (i.e. $T < 7300$ K) and most confirmed progenitor stars are red supergiants (as in Smartt 2015). This observation is consistent with predictions of star formation and stellar evolution, which suggest that SNe from lower mass and redder stars should be more common.

It is therefore of enormous scientific value when SN progenitor stars are detected at the extremes of observed colour and luminosity distributions, as these stars can both probe unusual SN explosions found in nature and challenge interpretations of stellar evolution and SN physics. In particular, several Type IIb supernovae (SNe IIb; SNe with strong hydrogen lines at early times that are relatively weak at later times, implying a thin hydrogen envelope) have been discovered with progenitor-star detections, which appear to span the stellar temperature range from red to blue supergiants (see e.g. SNe 1993J, 2008ax, 2011dh, and 2013df; Aldering et al. 1994; Crockett et al. 2008; Maund et al. 2011; Van Dyk et al. 2014). Examples such as SN 1993J challenge single-star evolution models as their progenitor-star colours cannot be matched to the end points of most plausible evolutionary tracks (Aldering et al. 1994). This discovery has led to the interpretation that at least some SNe IIb come from binary-star systems where mass from the progenitor star has been stripped by a companion (Nomoto et al. 1993; Woosley et al. 1994; Fox et al. 2014).

★ Email: cdkilpat@ucsc.edu

In this paper, we discuss SN 2016gkg[1] discovered in NGC 613. This SN was discovered by Buso & Otero (2016) on 2016 September 20.18 (all dates presented herein are UT) and reported in a subsequent detection on September 20.54 by Tonry et al. (2016). Within the nine hours between these detections, the SN appeared to have brightened by ∼3 mag. Jha, Van Wyk & Vaisanen (2016) reported a spectroscopic confirmation on September 21.9 that SN 2016gkg was a young Type II SN. Subsequent high-resolution spectroscopy on September 25.33 by Andrews & Smith (2016) found broad Hα emission with P-Cygni features that matched SN 1987A around peak magnitude. On September 28.56, Van Dyk et al. (2016) found in low-resolution spectroscopy that SN 2016gkg more closely resembled an SN IIb. Here, we present early-time imaging of SN 2016gkg and a new spectral epoch. We discuss detailed astrometry of the SN at early times, which demonstrates that the position of the SN is consistent with a blue source detected in archival *Hubble Space Telescope* (*HST*) Wide Field Planetary-Camera 2 (WFPC2) imaging. We fit the magnitudes derived from this source to stellar spectra and demonstrate that the best match is an A0 Ia star. Based on comparison to single and binary stellar evolution tracks, we show that this star most likely evolved in a binary system. Finally, we analyse the early-time light curve of SN 2016gkg, which rose rapidly in luminosity within a day after discovery, consistent with predictions of the cooling phase after shock break-out. We show that the stellar radius derived from this light curve is consistent with the radius of the detected progenitor star. Throughout this paper, we assume a Tully–Fisher distance to NGC 613 of 26.4 ± 5.3 Mpc, with a corresponding distance modulus of 32.11 ± 0.44 (Nasonova, de Freitas Pacheco & Karachentsev 2011), and Milky Way extinction of $A_V = 0.053$ (Schlafly & Finkbeiner 2011).

2 OBSERVATIONS

2.1 Archival data

We obtained archival imaging of NGC 613 from the *HST* Legacy Archive[2] from 2001 August 21 (Cycle 10, Proposal ID 9042, PI Stephen Smartt). The *HST*+WFPC2 data consisted of two frames each of *F*450*W*, *F*606*W*, and *F*814*W* totalling 2 × 160 s per filter. These data had been combined and calibrated by the Canadian Astronomical Data Centre using the latest calibration software and reference files, including corrections for bias, dark current, flat-fielding, and bad pixel masking. The images had been combined using the IRAF[3] task `MultiDrizzle` that performs automatic image registration, cosmic ray rejection, and final image combination using the `Drizzle` task. We performed photometry on these final, calibrated images in each filter using the DOLPHOT[4] stellar photometry package. Finally, we combined the images in all three filters using the `MultiDrizzle` task, weighting each image by the inverse-variance of emission-free regions in order to produce a reference image with the highest signal-to-noise (S/N) for each point source. This image is shown in Fig. 1.

We also obtained post-explosion photometry of SN 2016gkg recorded from Buso & Otero (2016), Nicholls et al. (2016), Tonry et al. (2016), and Chen et al. (2016). These data included observations from the All Sky Automated Survey for SuperNovae (ASAS-SN), the Asteroid Terrestrial-impact Last Alert System (ATLAS), and *Swift*, as well as photometry from the 1-m telescope on Cerro Tololo, Chile, as part of the Las Cumbres Observatory Global Telescope Network (LCOGT). The early-time photometry is summarized in Table 1, which was obtained from Chen et al. (2016).

2.2 Adaptive optics imaging

We observed SN 2016gkg in K' band with the Near-Infrared Camera 2 (NIRC2) on the Keck-II 10-m telescope in conjunction with the adaptive optics (AO) system on 2016 September 22, as summarized in Kilpatrick et al. (2016). These data consisted of 30 individual frames each consisting of three co-adds of 10 s for an effective exposure time of 30 s per frame and 900 s total. The individual frames were corrected for pixel-to-pixel variations using a flat-field frame that was created from the science frames themselves, and then sky-subtracted. Images taken with NIRC2 have known optical distortions. Therefore, each of the individual frames was resampled to a corrected grid, using the coordinate distortions that are provided on the NIRC2 web site.[5] We masked each individual frame in order to remove bad pixels, cosmic rays, and additional image artefacts. Finally, we aligned the individual frames using an offset vector calculated from the position of the SN and combined the individual frames. In Fig. 1, we show the AO imaging along with the reference *HST* archival image.

2.3 Spectroscopy

A spectrum of SN 2016gkg was obtained on 2016 October 8 with the Goodman Spectrograph (Clemens, Crain & Anderson 2004) and the 4.1-m Southern Astrophysical Research Telescope (SOAR) on Cerro Pachón, Chile. We used the 1.07-arcsec slit in conjunction with the 400 l/mm grating for an effective spectral range of 4000–7050 Å on the blue side and 5000–9050 Å on the red side, and a single 1200-s exposure per side. A blocking filter (GG-455) was used in the red to minimize second-order scattering of blue light on to the CCD. During our observations, we aligned the slit with the centre of NGC 613 in order to simultaneously observe the SN and host galaxy. The SN was at an airmass of ∼1.01 at this time and chromatic atmospheric dispersion was minimal. Conditions were photometric at the time of observations with ∼0.8-arcsec seeing. We used IRAF to perform standard reductions on the two-dimensional images and optimal extraction of the one-dimensional blue and red side spectra. We performed wavelength calibration on these one-dimensional images using arc lamp exposures taken immediately after each spectrum. We derived a sensitivity function from a standard star obtained at similar airmass and in the same instrument configuration, and used this function to perform flux calibration. We dereddened the spectrum using the extinction quoted above and removed the recession velocity $v = 1480\ \mathrm{km\,s^{-1}}$, which is consistent with the velocity of the host galaxy. Finally, we combined the red and blue spectra into a single spectrum, which is presented in Fig. 2.

[1] This name was adopted from Tonry et al. (2016) and subsequent Astronomer's Telegrams.
[2] https://hla.stsci.edu/hla_faq.html
[3] IRAF, the Image Reduction and Analysis Facility, is distributed by the National Optical Astronomy Observatory, which is operated by the Association of Universities for Research in Astronomy under cooperative agreement with the National Science Foundation (NSF).
[4] http://americano.dolphinsim.com/dolphot/
[5] http://www2.keck.hawaii.edu/inst/nirc2/nirc2dewarp_positions.pro

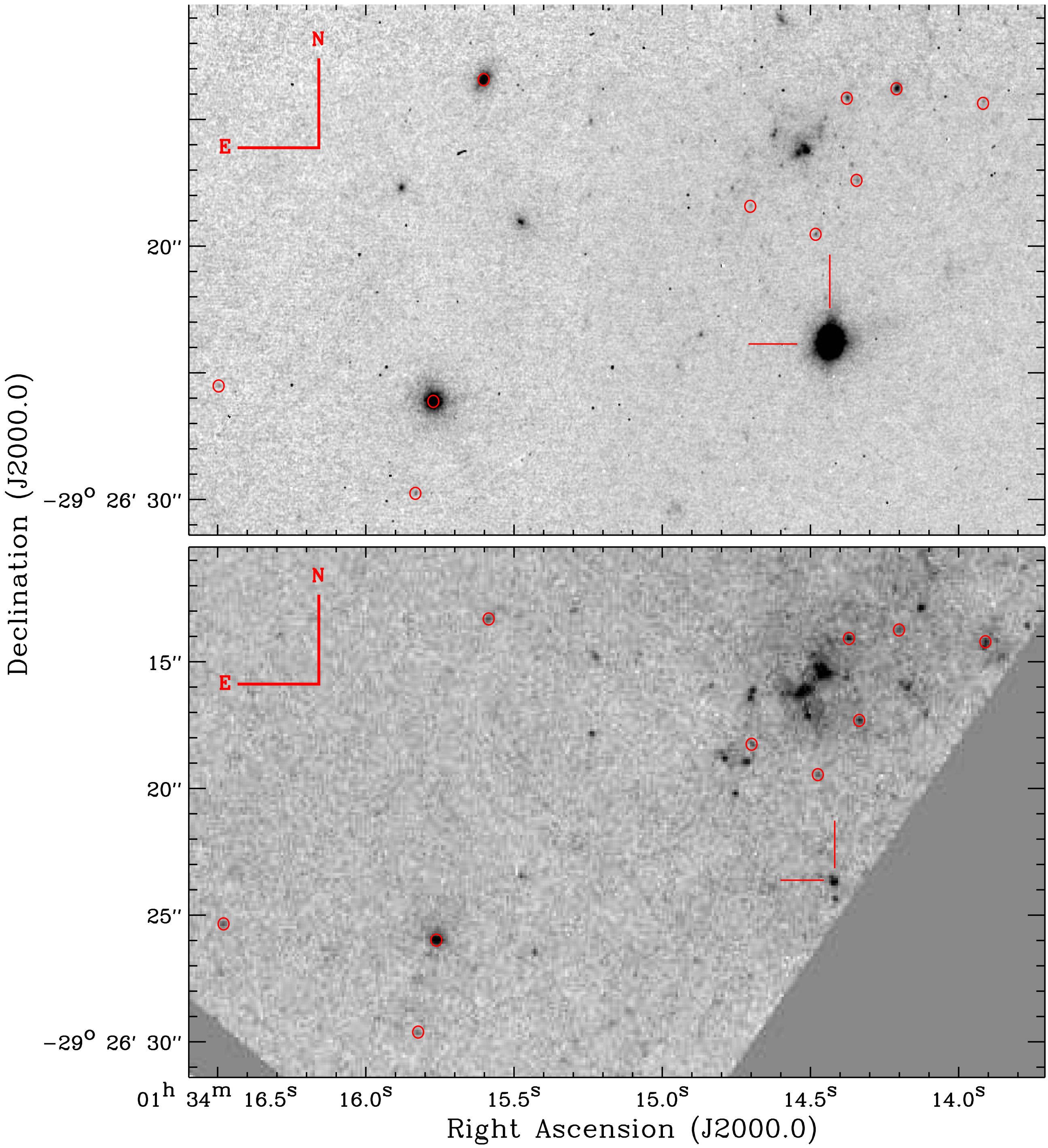

Figure 1. Upper panel: Keck NIRC2 AO K' imaging of SN 2016gkg. The SN is denoted and 10 point sources used for astrometry are circled in red. Bottom panel: *HST* WFPC2 *F*450*W*+*F*606*W*+*F*814*W* reference image used for astrometry. The progenitor star is denoted and the same 10 point sources from the NIRC2 image are circled in red.

3 RESULTS AND DISCUSSION

3.1 Spectrum of SN 2016gkg

In Fig. 2, we compare our spectrum of SN 2016gkg to spectra of the SNe IIb 1993J, 1997dd, and 2008ax (Matheson et al. 2000, 2001; Taubenberger et al. 2011). The comparison spectra have been dereddened and their recession velocities have been removed according to the extinction and redshift information provided in each reference. We indicate the relative epoch of each spectrum with respect to the explosion dates calculated for SNe 2016gkg, 1993J, and 2008ax (see below and Matheson et al. 2000; Taubenberger et al. 2011) and with respect to discovery date on 1997 August 26.18 for SN 1997dd (Nakano et al. 1997).

The comparison between these spectra, especially in He I λλ5876 and 7065 absorption, strongly suggests that SN 2016gkg is an SN

Table 1. Ultraviolet/optical photometry of SN 2016gkg.

UT date (from 2016 September 20)	Telescope	Filter	Magnitude	Uncertainty	Reference
0.1653	ASAS-SN	*V*	>17.36	–	(1)
0.2484	Buso & Otero	Clear	17.6	0.5	(2)
0.54	ATLAS	*o*	15.94	0.13	(3)
0.55	ATLAS	*o*	15.78	0.08	(3)
1.1398	Buso & Otero	Clear	14.5	0.2	(2)
1.2987	ASAS-SN	*V*	15.01	0.04	(1)
1.6569	*Swift*	UVW1	13.75	0.04	(4)
1.6588	*Swift*	*U*	13.97	0.04	(4)
1.6598	*Swift*	*B*	15.21	0.04	(4)
1.6608	*Swift*	UVW2	13.92	0.04	(4)
1.6645	*Swift*	*V*	15.09	0.05	(4)
1.7318	*Swift*	UVM2	13.70	0.14	(5)
2.1276	LCOGT	*B*	15.70	0.04	(4)
2.1289	LCOGT	*V*	15.54	0.03	(4)
2.1302	LCOGT	*g*	15.61	0.03	(4)
2.1315	LCOGT	*i*	15.65	0.04	(4)
2.1328	LCOGT	*r*	15.59	0.04	(4)
2.2884	ASAS-SN	*V*	15.73	0.05	(4)
2.3946	LCOGT	*B*	16.01	0.08	(4)
2.3959	LCOGT	*V*	15.84	0.06	(4)
2.3972	LCOGT	*g*	15.91	0.07	(4)
2.3998	LCOGT	*r*	15.85	0.08	(4)

References: (1) Nicholls et al. (2016), (2) Buso & Otero (2016), (3) Tonry et al. (2016), (4) Chen et al. (2016), (5) Chen (private communication).

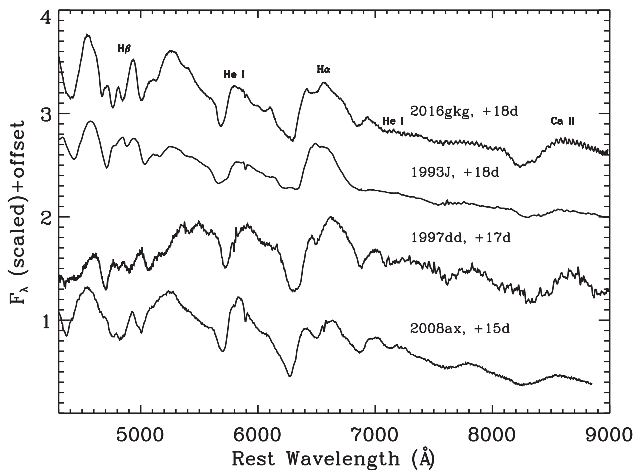

Figure 2. SN 2016gkg spectrum with the day relative to explosion (+##d) of observation given in black. For comparison, we also plot the SNe IIb 1993J, 1997dd, and 2008ax at a similar epoch relative to explosion (to discovery for 1997dd; Matheson et al. 2000, 2001; Taubenberger et al. 2011). All spectra have been dereddened and their recession velocities have been removed given the parameters provided in each reference. We indicate prominent emission and absorption features in these SN IIb spectra, including Hα, Hβ, He I $\lambda\lambda$5876 and 7065, and the Ca II infrared triplet.

IIb and was around or slightly before peak magnitude (or secondary peak as in SN 1993J; Benson et al. 1994). The development of these He I features appears to be more rapid than in SN 1993J based on our estimated explosion date for SN 2016gkg (Section 3.5) and is more similar to SN 2008ax at this epoch. In addition, Hα is not a dominant emission feature in SN 2016gkg at this epoch, implying that the initial hydrogen emission may be fading relative to the continuum level. Our spectrum is very similar to the early spectrum of SN 1997dd, where a distinct 'notch' developed in the Hα line, likely due to the P-Cygni profile of He I λ6678 before He absorption had fully developed (e.g. Matheson et al. 2001). We note additional similarities to SN 1997dd, which was identified early as a peculiar Type II SN with weak Hα emission (Suntzeff & Phillips 1997), as with SN 2016gkg in analysis by Jha et al. (2016).

As we mention in Section 2, we aligned the slit of the Goodman Spectrograph to obtain a spectrum of NGC 613 simultaneously with SN 2016gkg. Analysis of the host-galaxy emission line ratio

$$\log R_{23} = \frac{I_{[\mathrm{O\,II}]\lambda3727} + I_{[\mathrm{O\,III}]\lambda4959} + I_{[\mathrm{O\,III}]\lambda5007}}{I_{\mathrm{H}\beta}} \tag{1}$$

using the calibration in Kobulnicky & Kewley (2004) suggests that NGC 613 has $12 + \log(\mathrm{O/H}) = 8.61 \pm 0.15$ with an implied metallicity of $Z = 0.012 \pm 0.004$. This value is slightly sub-solar $[12 + \log(\mathrm{O/H})_{\odot} = 8.7]$, although it agrees with the solar value to within our error bars. We adopt $Z = 0.012$ for subsequent analysis of the SN 2016gkg progenitor star.

3.2 Astrometry of the AO imaging and *HST* point source

We performed relative astrometry on the AO image and composite *HST* image using the 10 common sources circled in both frames (Fig. 1). The positions derived for these 10 sources were determined using DOLPHOT in each frame and image registration was carried out on the AO image using the IRAF tasks `ccmap` and `ccsetwcs`. We used default parameters for `ccmap`, which fit pixel coordinates from the stars identified in our AO imaging to a tangent plane projection of the right ascensions and declinations of the same stars in the *HST* image. We used a general geometric fit, which included terms for linear shift, rotation, and distortion. An astrometric uncertainty was calculated from the standard deviation of the best-fitting projection in right ascension and declination, with $\sigma_\alpha = 0.023$ arcsec and $\sigma_\delta = 0.036$ arcsec. The position of the progenitor star in the *HST* reference image is $\alpha = 1^{\mathrm{h}}34^{\mathrm{m}}14\overset{\mathrm{s}}{.}418$, $\delta = -29°26'23\overset{''}{.}83$ and is detected with S/N = 5.8 for an astrometric precision of 0.052 arcsec. Relative astrometry from the AO image suggests that the position of SN 2016gkg is $\alpha = 1^{\rm h}34^{\rm m}14\overset{\rm s}{.}424$, $\delta = -29°26'23\overset{''}{.}82$ for an offset of $\Delta\alpha = +0.05$ arcsec, $\Delta\delta = -0.01$ arcsec. The combined offset is well within the uncertainty from *HST* astrometry and relative astrometry (0.89σ; astrometric uncertainty from the position of SN 2016gkg is negligible), and we conclude that the positions of these objects agree with each other. This evidence strongly suggests that the point source detected in archival *HST* imaging is the progenitor star of SN 2016gkg.

We estimate the probability of a chance coincidence in the *HST* image by noting that there are a total of 12 point sources with S/N > 3 in the *HST* image from Fig. 1. The 3σ error ellipse for the *HST* reference image has a solid angle of approximately 0.64 arcsec^2, which implies that ~7.6 arcsec^2 or 0.12 per cent of the *HST* archival image has a point source that is close enough to be associated with that region. This value represents the probability that the detected point source is a chance coincidence, and we find that it is extremely unlikely that the blue point source was aligned with the position of the SN by chance.

3.3 Photometric classification of the progenitor star

From our photometric analysis of the SN 2016gkg progenitor star, we obtained ST (Vega) magnitudes $m_{F450W} = 22.93(23.41) \pm 0.47$, $m_{F606W} = 23.40(23.08) \pm 0.33$, $m_{F814W} = 24.56(23.29) \pm 0.59$ mag. We note that our $F606W$ magnitude for this source is discrepant from Tartaglia et al. (2016) as measured in HSTPHOT and DOLPHOT, although this value and our $F450W$ magnitude agree with the values reported in the *Hubble* Source Catalog[6] ($F450W = 23.85 \pm 0.08$ mag, $F606W = 23.34 \pm 0.05$ mag in the Vega magnitude system). In addition, our $m_{\rm F450W}$ and $m_{\rm F814W}$ magnitudes are consistent with Tartaglia et al. (2016).

Although, Tartaglia et al. (2016) report the detection of a second point source near the source we have identified, our DOLPHOT analysis does not recover it. It is possible that additional faint sources or background emission contaminates our photometry, although the sharpness recovered from DOLPHOT for the reported source is −0.043, consistent with a single star. It is more likely that any additional sources are below the level of significance for a detection, given our estimate of the measurement uncertainties.

For the *HST* photometry reported above, we corrected for interstellar extinction using equations 3a, 3b, 4a, and 4b in Cardelli, Clayton & Mathis (1989) with $R_V = 3.1$ (used for all photometry herein). We then used these magnitudes to determine the spectral type of the SN 2016gkg progenitor star by comparing to stellar spectra from Pickles (1998). Fitting the redshift-corrected flux density to stellar spectra convolved with the WFPC2 transmission curves for the $F450W$, $F606W$, and $F814W$ filters, we determined the best-fitting stellar spectrum and thus the temperature and bolometric correction by minimizing the χ^2 of the observed and model flux densities. In Fig. 3, we show the best-fitting stellar spectrum in black along with the stellar spectra with the lowest (red) and highest (blue) implied temperatures that were within $\Delta\chi^2/\chi^2_{\rm min} = 1$ of the minimum χ^2. The implied best-fitting temperature and bolometric correction are $T = 9500^{+6100}_{-2900}$ K and ${\rm BC}_V = -0.30^{+0.37}_{-0.88}$ mag. These values correspond to a spectral class of A0.

From the best-fitting stellar spectra, the implied flux density in Johnson V band is $7.2^{+3.2}_{-2.3} \times 10^{-19}$ erg s^{-1} cm^{-2} Å^{-1} or

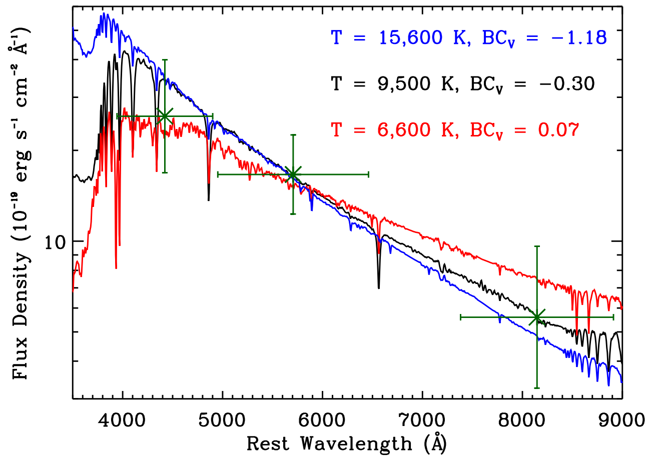

Figure 3. *HST* archival photometry from the SN 2016gkg progenitor star. The wavelength uncertainty of each point represents the width of the corresponding WFPC2 filter. Each point has been corrected for extinction and the recessional velocity of NGC 613 has been removed from the effective wavelength. Overplotted are the best-fitting (black) and $\Delta\chi^2/\chi^2_{\rm min} = 1$ (red/blue) stellar spectra obtained from Pickles (1998). We indicate the temperature and bolometric correction of each stellar spectrum in the upper-right of the panel.

$m_V = 24.3 \pm 0.4$ mag (implying the best-fitting stellar type is A0 Ia), which suggests that the overall bolometric magnitude is $m_{\rm bol} = 24.0^{+0.54}_{-0.97}$ mag. The luminosity of the SN 2016gkg progenitor star is therefore $\log(L/{\rm L}_\odot) = 5.14^{+0.22}_{-0.39}$ with an implied radius of $\log(R/R_\odot) = 2.14^{+0.29}_{-0.59}$. Along with the temperature we infer, these values are in agreement with those inferred from Tartaglia et al. (2016) for Source A, the brighter of two sources resolved in pre-explosion *HST* imaging near the putative location of SN 2016gkg. In addition, we note that these values are remarkably similar to the progenitor-star model for SN 2008ax in Crockett et al. (2008) where the authors found the photometry was well-fitted by a B8 to early K supergiant combined with an M4 supergiant, the former having $\log(L/{\rm L}_\odot) = 5.1$, $T = 8900$ K (see also Smartt 2015). In our discussion of the SN 2016gkg spectrum above, we emphasize this comparison with SN 2008ax at 15 d after explosion.

3.4 Matching the SN 2016gkg progenitor star to stellar evolution tracks

In order to constrain the zero-age main-sequence mass ($M_{\rm ZAMS}$) and evolutionary path of an SN progenitor star, it is necessary to compare the luminosity and temperature derived from photometry to model evolutionary tracks. This analysis has been done for a number of SNe IIb including SN 1993J (Podsiadlowski 1993), SN 2008ax (Crockett et al. 2008), SN 2011dh (Maund et al. 2011; Van Dyk et al. 2011; Bersten et al. 2012), and SN 2013df (Van Dyk et al. 2014). Here, we analyse the temperature and luminosity derived for SN 2016gkg to single- and binary-star models on the Hertzsprung–Russell (HR) diagram and make comparisons to these example SN IIb progenitor stars.

3.4.1 Single-star models

Single-star models were obtained from Brott et al. (2011) for $M_{\rm ZAMS} = 5$–60-M$_\odot$ stars. We examined models with metallicity $Z = 0.0088$, which was the closest set to the observed metallicity of NGC 613. We overplot these models with the observed parameters

[6] https://archive.stsci.edu/hst/hsc/

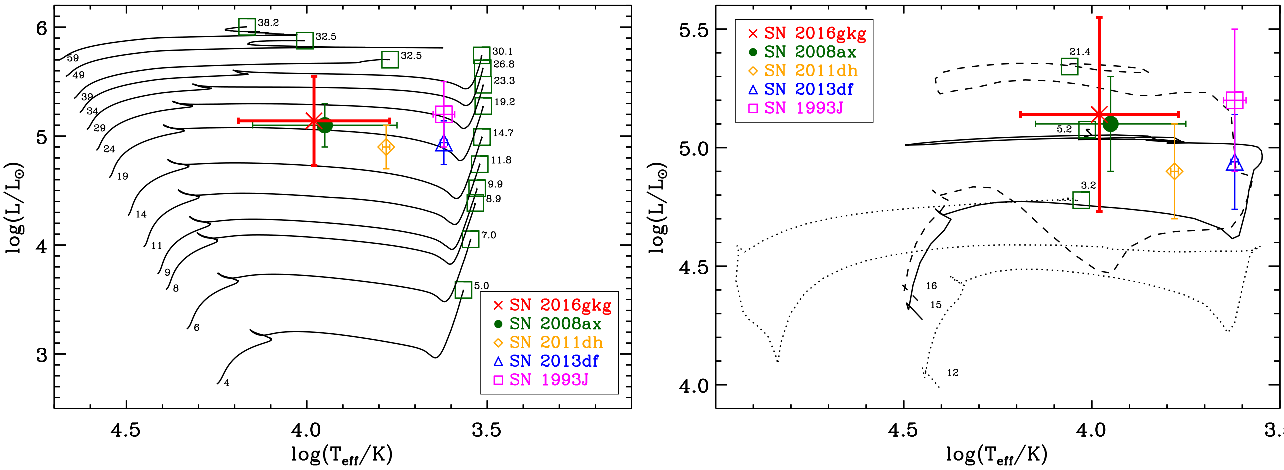

Figure 4. Left: Single-star evolutionary tracks plotted on the HR diagram with the inferred luminosity and temperature from SN 2016gkg overplotted. We also indicate the inferred luminosities and temperatures from the SNe IIb 2008ax, 2011dh, 2013df, and 1993J (Aldering et al. 1994; Crockett et al. 2008; Maund et al. 2011; Van Dyk et al. 2011, 2014). The initial mass and final mass of the modelled star are given near the start and end points of each evolutionary track (the latter is indicated with a square). As we demonstrate, no single-star evolutionary track terminates near the inferred luminosity and temperature of the SN 2016gkg – or any other SN IIb – progenitor star. Right: same as the left-hand panel but for the binary-star models that terminate at values in agreement with the inferred luminosity and temperature for SN 2016gkg (as discussed in Section 3.4.2). The best-fitting model has an initial stellar mass of $M = 15\,\mathrm{M}_\odot$ with a 1.5-$\mathrm{M}_\odot$ companion. The initial period is 1000 d and the primary star explodes with $M = 5.2\,\mathrm{M}_\odot$. Two additional examples with initial masses $12\,\mathrm{M}_\odot$ (8.4-$\mathrm{M}_\odot$ initial mass companion, 160-d period) and $16\,\mathrm{M}_\odot$ (14.4-$\mathrm{M}_\odot$ initial mass companion, 6.3-d period) are shown with dotted and dashed lines, respectively. All of these models agree with the inferred luminosity and temperature of SN 2016gkg.

of the SN 2016gkg progenitor star on the HR diagram in Fig. 4. As we demonstrate, there are no single-star models that are consistent with ending their evolutionary tracks near the predicted luminosity and temperature values.

We find that it is extremely unlikely that SN 2016gkg originated from a single star. Woosley & Heger (2007) and Sukhbold et al. (2016) have found that, for stars with $M_{\mathrm{ZAMS}} > 30\,\mathrm{M}_\odot$, the pre-SN iron core is too large for an SN to be successful. Moreover, mass-loss is sufficiently strong so that most of these stars lose their entire hydrogen envelopes and are thought to end their evolution as Wolf–Rayet stars, implying that the subsequent SN would be Type Ib or Ic. SNe IIb require progenitor stars with extended low-mass hydrogen envelopes (Podsiadlowski 1993; Woosley et al. 1994; Elmhamdi et al. 2006), and any single-star model for such a system would require finely tuned mass-loss that would otherwise fail to reproduce the observed range in SN IIb light curves, spectra, and progenitor stars. While the single-star scenario could describe a minority of SNe IIb, it is likely that the majority of these systems come from binary-star systems such as the one observed towards SN 1993J (Maund et al. 2004; Fox et al. 2014).

3.4.2 *Binary-star models*

We examine evolutionary tracks involving binary stars in order to assess the plausibility of these systems as possible progenitor stars for SN 2016gkg. We obtained our binary-star evolutionary tracks from the Binary Population and Spectral Synthesis (BPASS) code as described in Eldridge & Stanway (2009). These models provide a range of metallicities ($Z = 0.001$–0.040), primary-star masses ($M/\mathrm{M}_\odot = 0.1$–300), mass ratios ($q = 0.1$–0.9), and initial periods [$\log(P/1\,\mathrm{d}) = 0$–$4$]. We fixed the metallicity of the binary-star models to $Z = 0.010$ in order to provide the best match to the observed metallicity of NGC 613. Otherwise, we examined the full range of parameters provided by BPASS.

For our fitting scheme, we looked for binary-star models that produced a primary star with terminal luminosity and temperature that minimized

$$\chi^2 = \frac{(T_{\mathrm{model}} - T_{\mathrm{SN\,2016gkg}})^2}{\sigma^2_{T_{\mathrm{SN\,2016gkg}}}} + \frac{(L_{\mathrm{model}} - L_{\mathrm{SN\,2016gkg}})^2}{\sigma^2_{L_{\mathrm{SN\,2016gkg}}}}. \quad (2)$$

Overall, we found that 107 out of 5565 BPASS models terminated with primary-star luminosity and temperature within our measurement uncertainties for the SN 2016gkg progenitor star. Of these models, the χ^2 ranged from 0.11 to 4.01 with a median value of 1.05. In Fig. 4, we show the stellar evolution of the best-fitting binary-star model on the HR diagram along with the inferred luminosity and temperature of the SN 2016gkg progenitor star. The primary star has an initial mass of $15\,\mathrm{M}_\odot$ while the secondary (accreting) star has an initial mass of $1.5\,\mathrm{M}_\odot$ and an initial orbital period of 1000 d. We note in Fig. 4 that the pre-explosion mass of the best-fitting star is $M = 5.2\,\mathrm{M}_\odot$. The hydrogen that remains in the envelope from this best-fitting model is $5 \times 10^{-3}\,\mathrm{M}_\odot$, which agrees with models of SNe IIb (Dessart et al. 2011).

If SN 2016gkg evolved from a binary-star system, it may be possible to detect the companion star in follow-up photometry after the SN has faded. The secondary star in our best-fitting binary-star model is intrinsically much fainter than the SN 2016gkg progenitor star. Accounting for distance modulus and extinction, its expected brightness in *F*300*W* is 25.9 mag. It may be feasible to search for such a companion with sufficiently deep imaging.

3.5 Modelling the early-time light curve of SN 2016gkg

The early-time light curve of any SN can yield important information about the progenitor star when shock break-out is observed. For SNe other than SNe II-P, observations of this phase are extremely scarce as their progenitor stars are thought to have less extended envelopes, which implies a fast rise and decline in the early-time light curve. In the rare cases where this phase is observed, hydrodynamical models can constrain the radius of the progenitor star, as larger

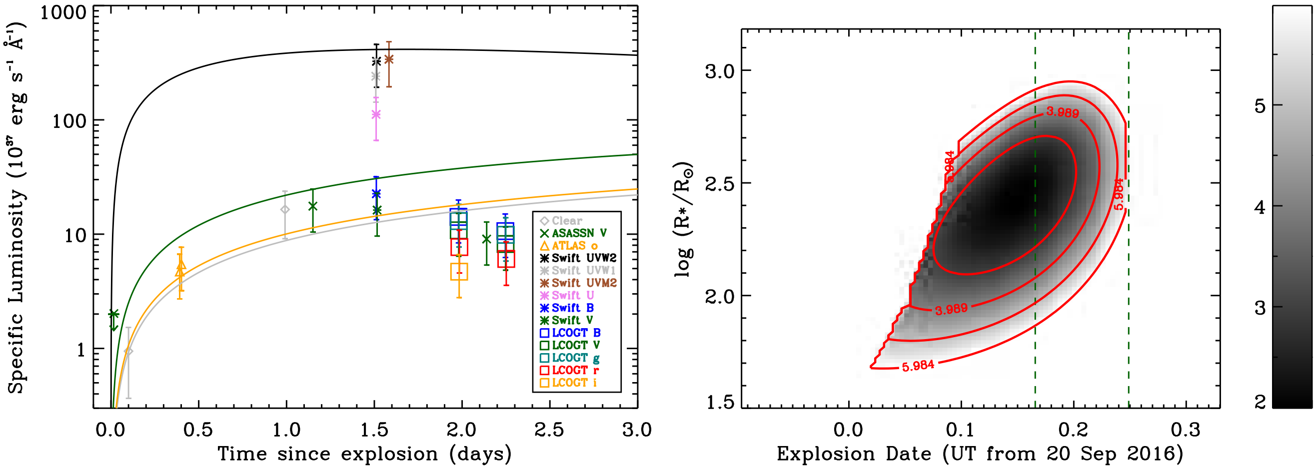

Figure 5. Left: early-time light curve of SN 2016gkg as discussed in Section 3.5 and referenced in Nicholls et al. (2016) and Tonry et al. (2016). The data are plotted in terms of specific luminosity (i.e. $L_\lambda = 4\pi D^2 f_\lambda$). Overplotted are light curves of the cooling phase that follows shock break-out based on models provided in Rabinak & Waxman (2011) and for a range of filter transmission curves including 'Clear' (grey), ATLAS *o* (orange), ASAS-SN *V* (green), and *Swift* UVW2 (black). These models use the best-fitting explosion time and progenitor-star radius derived from photometry within 1.5 d of the initial ASAS-SN *V*-band upper limit (indicated on the left with an arrow). Other parameters used to derive these light curves are described in Section 3.5. Right: χ^2 for the range of model parameters used to derive the light curves on the left. We have overplotted two dashed lines to indicate the time of the ASAS-SN *V*-band upper-limit (2016 September 20.1653) and the first photometry point (2016 September 20.2484), which place the strongest constraints on the explosion date.

stars tend to have hotter effective temperatures with a more luminous initial peak while smaller stars tend to appear cooler. In our analysis of the early-time light curve, we use models derived from Rabinak & Waxman (2011) for a star with a hydrogen envelope density profile $\rho \approx (1 - r/R_*)^3$ (where R_* is the stellar radius). In general, we assume that the progenitor star has a blackbody colour temperature 20 per cent larger than the photospheric temperature and typical Thomson scattering opacity $\kappa = 0.34\,\mathrm{cm^2\,g^{-1}}$. Rabinak & Waxman (2011) and Bersten et al. (2012) demonstrated that these assumptions are good approximations of more detailed models for $t < 1$ d after explosion.

In order to calculate the radius of the progenitor star, we must make assumptions about the explosion energy and ejecta mass of SN 2016gkg. These parameters are well-known for the SN IIb 1993J, which we have demonstrated is a good match for SN 2016gkg at the epoch of our spectroscopic observation. We employ parameters for an SN 1993J-like explosion with ejecta mass, $M_{\rm ej} = 2.6\,\mathrm{M_\odot}$, and explosion energy, $E = 10^{51}$ erg (Woosley et al. 1994; Young, Baron & Branch 1995). Using these parameters, we fit specific luminosity to the model at a time t since explosion with

$$L_\lambda = 0.234\mu r^2 \frac{(hc/\lambda)^5}{\exp\left(hc/\lambda T\right) - 1} \tag{3}$$

$$r = 3.3 \times 10^{14} \frac{E_{51}^{0.39}\kappa_{0.34}^{0.11}}{(M_{\rm ej}/\mathrm{M_\odot})^{(0.28)}} t_5^{0.78}\ \mathrm{cm} \tag{4}$$

$$T = 1.6 \frac{E_{51}^{0.016} R_{*,13}^{1/4}}{(M_{\rm ej}/\mathrm{M_\odot})^{0.033}\kappa_{0.34}^{0.27}} t_5^{-0.47}\ \mathrm{eV}, \tag{5}$$

where $E = E_{51}10^{51}$ erg, $\kappa = \kappa_{0.34}0.34\,\mathrm{cm^2\,g^{-1}}$, $t = t_5 10^5$ s, $R_* = R_{*,13}10^{13}$ cm, and $\mu = 1.14 \times 10^{12}\,\mathrm{cm^{-3}\,s^{-1}\,K^{-4}}$ (i.e. the ratio of the radiation constant to the Planck constant). As we have noted, this model breaks down for times significantly (e.g. > 1 d) after explosion. Therefore, in determining the explosion date and stellar radius, we fit only photometry within 1.5 d of the ASAS-SN *V*-band limit on 2016 September 20.165. These include the discovery magnitudes and follow-up photometry from Nicholls et al. (2016) and Tonry et al. (2016).

We constructed a range of models using the equations above and convolved the specific luminosity with the filter transmission curves. In Fig. 5, we show our best-fitting model for a range of filters, including ASAS-SN *V*, ATLAS *o*, the 'Clear' filter, and the *Swift* UVW2. Our best-fitting model corresponds to a stellar radius of $\log(R/R_\odot) = 2.41^{+0.40}_{-0.58}$ and an explosion date of t_0 = 2016 September $20.15^{+0.08}_{-0.10}$. Our range of best-fitting parameters is also displayed in Fig. 5 with contours representing χ^2 overplotted.

The early-time light curve agrees with all of the photometry within 1.5 d of explosion to within the 1σ uncertainties. After this point, there is general disagreement between the model and observed magnitudes, especially at redder wavelengths where the model overpredicts the specific luminosities and does not turn over as quickly as the observed light curve. This disagreement is likely caused by our assumption of a constant Thomson-like opacity, independent of time and spatial coordinate in the model star. In more realistic models, the opacity is sensitive to the ionization state of the model star and decreases as hydrogen in the envelope recombines. However, good agreement can be found at early times between this model and the SN 1987A light curve (Rabinak & Waxman 2011) and the SN 2011dh light curve (Bersten et al. 2012) where most of the hydrogen envelope is ionized. Therefore, we are confident that the explosion date and progenitor-star radius inferred from this model is an accurate representation of the light curve.

4 CONCLUSIONS

We describe new astrometric and photometric analysis of the SN 2016gkg progenitor star as well as optical photometry and spectroscopy of the SN itself. Our analysis yields new insight into SN 2016gkg and we find the following.

(i) Astrometric analysis of our AO imaging indicates the SN position is consistent with the position of a blue point source in *HST* imaging. Fitting the photometry of this source, we find the best-fitting stellar model to be an A0 Ia star with $\log(L/L_{\odot}) = 5.14^{+0.22}_{-0.39}$ and $T = 9500^{+6100}_{-2900}$ K and implied radius of $\log(R/R_{\odot}) = 2.14^{+0.29}_{-0.59}$.

(ii) Based on the best-fitting luminosity and temperature of the SN 2016gkg progenitor star, we find that single-star models do not terminate with the inferred properties. Rather, we find that binary-star models are required to produce evolutionary tracks with primary-star terminal properties that match the SN 2016gkg progenitor star. The best-fitting binary-star model involves a primary star with $M_{\mathrm{ZAMS}} = 15\,\mathrm{M}_{\odot}$ and a secondary with $M_{\mathrm{ZAMS}} = 1.5\,\mathrm{M}_{\odot}$. With sufficiently deep imaging, it may be possible to detect the secondary star once the SN has faded significantly.

(iii) We fit analytic models of the cooling phase that follows shock break-out to the specific luminosity observed from SN 2016gkg. These models are sensitive to both the explosion date and radius of the progenitor star. Our best-fitting explosion date and progenitor-star radius are $t_0 = 2016$ September $20.15^{+0.08}_{-0.10}$ and $\log(R/R_{\odot}) = 2.41^{+0.40}_{-0.58}$. The latter value is in agreement with the radius fit to the progenitor star from pre-explosion photometry.

ACKNOWLEDGEMENTS

We would like to thank John Tonry for providing data from ATLAS, as well as Dan Kasen, Josiah Schwab, Enrico Ramirez-Ruiz, and Stan Woosley for their helpful discussions. We also thank Marc Kassis for his assistance with Keck data acquisition, Nathan Smith and Jennifer Andrews for discussing spectroscopy of SN 2016gkg, and Subo Dong and Ping Chen for assistance with *Swift* photometry of SN 2016gkg.

The UCSC group is supported in part by NSF grant AST-1518052 and from fellowships from the Alfred P. Sloan Foundation and the David and Lucile Packard Foundation to RJF.

Some of the data presented herein were obtained at the W. M. Keck Observatory, which is operated as a scientific partnership among the California Institute of Technology, the University of California, and NASA. The observatory was made possible by the generous financial support of the W. M. Keck Foundation. We wish to recognize and acknowledge the cultural significance that the summit of Mauna Kea has within the indigenous Hawaiian community. We are most fortunate to have the opportunity to conduct observations from this mountain.

Some of our photometry of SN 2016gkg comes from All Sky Automated Survey for SuperNovae (ASAS-SN), the Asteroid Terrestrial-impact Last Alert System (ATLAS), *Swift*, and the Las Cumbres Observatory Global Telescope Network (LCOGT). The *Hubble Space Telescope* (*HST*) is operated by NASA/ESA. Some of our analysis is based on data obtained from the *HST* archive operated by STScI. Our analysis is based in part on observations obtained at the Southern Astrophysical Research (SOAR) telescope, which is a joint project of the Ministério da Ciência, Tecnologia, e Inovação (MCTI) da República Federativa do Brasil, the US National Optical Astronomy Observatory (NOAO), the University of North Carolina at Chapel Hill (UNC), and Michigan State University (MSU). This work has made use of the following facilities: Keck (NIRC2); SOAR (Goodman).

REFERENCES

Aldering G., Humphreys R. M., Richmond M., 1994, AJ, 107, 662
Andrews J., Smith N., 2016, Astron. Telegram, 9562, 1
Arnett W. D., 1987, ApJ, 319, 136
Arnett W. D., Bahcall J. N., Kirshner R. P., Woosley S. E., 1989, ARA&A, 27, 629
Benson P. J. et al., 1994, AJ, 107, 1453
Bersten M. C. et al., 2012, ApJ, 757, 31
Brott I. et al., 2011, A&A, 530, A115
Buso V., Otero S., 2016, vsnet-alert 20188
Cardelli J. A., Clayton G. C., Mathis J. S., 1989, ApJ, 345, 245
Chen P. et al., 2016, Astron. Telegram, 9529, 1
Clemens J. C., Crain J. A., Anderson R., 2004, in Moorwood A. F. M., Iye M., eds, Proc. SPIEConf. Ser. Vol. 5492, Ground-based Instrumentation for Astronomy. SPIE, Bellingham, p. 331
Crockett R. M. et al., 2008, MNRAS, 391, L5
Dessart L., Hillier D. J., Livne E., Yoon S.-C., Woosley S., Waldman R., Langer N., 2011, MNRAS, 414, 2985
Eldridge J. J., Stanway E. R., 2009, MNRAS, 400, 1019
Elmhamdi A., Danziger I. J., Branch D., Leibundgut B., Baron E., Kirshner R. P., 2006, A&A, 450, 305
Fox O. D. et al., 2014, ApJ, 790, 17
Jha S. W., Van Wyk V., Vaisanen P., 2016, Astron. Telegram, 9528, 1
Kilpatrick C. D. et al., 2016, Astron. Telegram, 9536, 1
Kobulnicky H. A., Kewley L. J., 2004, ApJ, 617, 240
Matheson T. et al., 2000, AJ, 120, 1487
Matheson T., Filippenko A. V., Li W., Leonard D. C., Shields J. C., 2001, AJ, 121, 1648
Mauerhan J. C. et al., 2013, MNRAS, 430, 1801
Maund J. R., Smartt S. J., Kudritzki R. P., Podsiadlowski P., Gilmore G. F., 2004, Nature, 427, 129
Maund J. R. et al., 2011, ApJ, 739, L37
Morris T., Podsiadlowski P., 2007, Science, 315, 1103
Nakano S., Aoki M., Garnavich P., Kirshner R., Stanek K., 1997, IAU Circ., 6724, 1
Nasonova O. G., de Freitas Pacheco J. A., Karachentsev I. D., 2011, A&A, 532, A104
Nicholls B. et al., 2016, Astron. Telegram, 9521, 1
Nomoto K., Suzuki T., Shigeyama T., Kumagai S., Yamaoka H., Saio H., 1993, Nature, 364, 507
Pickles A. J., 1998, PASP, 110, 863
Podsiadlowski P., 1993, Space Sci. Rev., 66, 439
Rabinak I., Waxman E., 2011, ApJ, 728, 63
Schlafly E. F., Finkbeiner D. P., 2011, ApJ, 737, 103
Smartt S. J., 2015, PASA, 32, e016
Smartt S. J., Eldridge J. J., Crockett R. M., Maund J. R., 2009, MNRAS, 395, 1409
Sukhbold T., Ertl T., Woosley S. E., Brown J. M., Janka H.-T., 2016, ApJ, 821, 38
Suntzeff N., Phillips M., 1997, IAU Circ., 6725, 1
Tartaglia L. et al., 2016, ApJ, preprint (arXiv:1611.00419)
Taubenberger S. et al., 2011, MNRAS, 413, 2140
Tonry J., Denneau L., Stalder B., Heinze A., Sherstyuk A., Rest A., Smith K. W., Smartt S. J., 2016, Astron. Telegram, 9526, 1
Van Dyk S. D. et al., 2011, ApJ, 741, L28
Van Dyk S. D. et al., 2014, AJ, 147, 37
Van Dyk S. D., Zheng W., Shivvers I., Filippenko A. V., Tucker B. E., Perley D. A., Smith N., 2016, Astron. Telegram, 9573, 1
Weiler K. W., Williams C. L., Panagia N., Stockdale C. J., Kelley M. T., Sramek R. A., Van Dyk S. D., Marcaide J. M., 2007, ApJ, 671, 1959
Woosley S. E., Heger A., 2007, Phys. Rep., 442, 269
Woosley S. E., Pinto P. A., Martin P. G., Weaver T. A., 1987, ApJ, 318, 664
Woosley S. E., Eastman R. G., Weaver T. A., Pinto P. A., 1994, ApJ, 429, 300
Young T. R., Baron E., Branch D., 1995, ApJ, 449, L51